LA-UR-19-29745
Approved for public release; distribution is unlimited.

Title: Extending Beryllium Strength Calibration To High Strain-rate Regimes

Author(s): Gafur, Jamil
Tourangeau, Eva Marie
Hickmann, Kyle Scott
Prime, Michael Bruce
Wendelberger, Joanne Roth

Intended for: Report

Issued: 2019-09-26

# Extending Beryllium Strength Calibration to High Strain-rate Regimes

Jamil Gafur[1], Eva Tourangeau[2], Kyle Hickmann[1],
Mike Prime[3], Joanne Wendelberger[2]

XCP-8[1], CCS-6[2], E-13[3]
Los Alamos National Laboratory
Los Alamos, NM

**Abstract**

Current calibration of the PTW strength model for beryllium is accomplished using fits to Hopkinson bar experiments. Unfortunately, Hopkinson bar tests on beryllium only allow for strain-rates of up to $5 * 10^3\, s^{-1}$. It has been shown previously that, in higher strain-rate experiments such as flyer-plate impact tests, this calibrated strength model causes simulations with beryllium to diverge from the observed response. In this work we use a particle swarm optimization algorithm to arrive at a better calibration of beryllium strength through fits to observed material responses during flyer-plate impact experiments. We show that the PTW strength model for beryllium can be tuned to provide a much better fit to flyer-plate responses. To mitigate the effect of this new calibration on fits to Hopkinson bar data we calibrate to flyer-plate impact data using only parameters within the medium strain-rate regime of the PTW model.

# Contents

# 1 Calibrating Constitutive Models Using High Impact Velocity Data

## 1.1 Introduction

Materials scientists at Los Alamos National Laboratory (LANL) validate physics models for materials. This is to test whether the model form sufficiently approximates the true behavior, when subjected to high-velocity impacts. The Preston-Tonks-Wallace (PTW) strength model relates a material's plastic deformation response, or its stress, to mechanical loading, or strain, in explosive loading scenarios. LANL would like to validate our calibrated PTW model across higher strain rate regimes. However, we currently have access to experimental data in a small range of regimes.

The PTW strength model is unlike most strength models because it has the ability to transitions between strain rate regimes. Many LANL researchers have taken different approaches to calibrate PTW at lower strain rates using Hopkinson bar and Quasi-Static experiments, their parameterizations agree at low strain rates, but diverge when extrapolated to higher strain rates.

Flyer-plate impact experiments allow the material being studied to be put under higher strain rates than found in Hopkinson bar and Quasi-Static experiments. These experiments measure the free surface velocity of a target material when struck forcefully by an impactor, subjecting the target to higher strain rates. Currently our calibrations to PTW fits poorly to flyer-plate data. Using multi-physics code developed at LANL to simulate the free surface velocity of targets struck in flyer-plate experiments, we can tune the parameters on the PTW strength model for Beryllium in these regimes to get better fits.

One complication with using flyer-plate data is the inability to measure strength directly, this allows for direct calibration of strength models. Due to the higher strain-rate impacts in flyer-plate experiments such a direct measurement is impossible. Though we cannot extract stress/strain data from flyer-plate experiments we can use the comparison between experimental and simulated free surface velocity to calibrate the strength model used in our calculation. We reduce the dimension of the parameter space by considering parameters in the PTW yield stress equation corresponding to strain rates from $10^4 - 10^6\, s^{-1}$, which are exercised in flyer impact tests. This has the advantage of reducing the effect of calibration to flyer-plate response on previous calibration to Hopkinson bar and Quasi-static data.

The reduced parameter space is traversed using a Particle Swarm Optimization algorithm (PSO), specifically the Gravitational Search Algorithm (GSA). In this report we show that the GSA allows us to reach an improved calibration of beryllium

strength to flyer-plate response while keeping its original fit to low strain rate data. The overall explanation of our experiment is explained in section 1.2

## 1.2 Experiment

Our current PTW strength model is calibrated to predicts the yield and saturation strength of a material for strain rates over $10^{-3} - 10^{4}\, s^{-1}$. From this, we can relate the strain applied to a material at a given pressure and temperature to its *equivalent plastic stress*. In order to calibrate our model to higher regimes we needed to gather stress/strain data across a range of strain rates, and compare the models current predictions to real data.

Obtaining measurements of stress in high-velocity experiments is done to study impact related problems. As previously stated this is impossible at strain-rates above $10^{4}\, s^{-1}$, which is well below the regime that flyer-plate experiments fall into. To mitigate this complication, velocimetry data from flyer-plate experiments act as an indirect means to calibrate the stress predictions of the PTW model.

An overview of the flyer-plate experiment is as follows; two plates are positioned in a near-vacuum inside a gun barrel. Explosives detonated behind the *flyer* plate launching it down the barrel towards the stationary *target* plate.

In such a high-speed impact experiment the impactors velocity is measured using radial shorting pins that are placed in the barrel before the point of impact. Piezo-electric pins fixed flush with the target face record the time of impact and the tilt of the impactor plate. A single VISAR probe directed at the face of the target collects the velocity measurement as the shockwave propagates through the target.

The speed of impact can reach anywhere from $10^{5}$ to $10^{9}$ m/s. As the impactor meets the target, the shock wave propagates through the target and forces it to first elastically then plastically deform. The propagation of particle velocity through the target over time is then recorded and used as experimental data.

In this work, we optimize the PTW yield stress parameters to calibrate the model for higher yield stress regimes. A brief literary review relating to the effect of yield stress at higher regimes will be reviewed in the next section. This review will be concerned particularly with the effect of optimizing the PTW yield stress parameter, the PTW strength and spall properties, and validating beryllium strength models.

## 1.3 Data

The data used in our study came from four flyer-plate experiments performed to examine the strength and damage behavior of S200F beryllium. There setup is as

follows: [1] [2]:

1. Performed on S-200F beryllium, vacuum hot-pressed from powder.
2. Impurity level below 1%.
3. Grain size about 11 $\mu m$. Specimens were machined such that the samples were loaded along the hot-pressing axis.
4. Texture in such samples has been modest at 2 or fewer multiples of random distribution.

The four types of experiments/shots that we had data on are shown in table 1

| Flyer plate experiments | | | |
|---|---|---|---|
| Shot/Experiment Name | Flyer | Impactor | Initial Velocity ($\mu$) |
| Shot $55-429$ | Beryllium | Beryllium | 0.071 |
| Shot $55-430$ | Beryllium | Beryllium | 0.1246 |
| Shot $55-432$ | Sapphire | Beryllium | 0.0654 |
| Shot $55-433$ | Tantalum | Beryllium | 0.1418 |
| Shot $55-436^*$ | Quartz | Beryllium | 0.02546 |

Table 1: Beryllium flyer-plate impact experiments. ($^*$ Shot $55-436$ included a Li-F window.) [3]

## 1.4 Literature

In this section we offer a brief literature review of modeling high strain-rate plastic deformation in metals. This is a vast field of research with a long history so we do not pretend that this review is exhaustive, instead we hope to offer the reader insight into the path that we have taken through the literature.

Adams et al. [3] detail the experimental setup and data collection processes of a series of flyer-plate impact experiments performed with beryllium targets. The experiments were performed in order to study strength and spall properties of S200F grade beryllium. Much work has been done on understanding the dynamic behavior of S200D or S200E grades, and less on the more pure and compact S200F grade. Two experiments used beryllium for both the impactor and target materials. Two other experiments in the paper were asymmetric, using alternately a sapphire and tantalum

impactor. Peak stresses were 5.56 and 10.20 $GPa$ for the two symmetric experiments and 7.66 and 19.25 $GPa$ for the sapphire and tantalum experiments. Across these four experiments, impact velocity ranged from 0.654 to 1.418 $\frac{mm}{\mu s}$. The data generated from [3] is the same data that is used in our experiments.

The paper from Preston, Tonks, and Wallace [4] provides details for the PTW strength model. This model will be explained in more detail in section 2. Unlike many strength models available the PTW model allows attempts to model a material's strength over a very large range of temperatures, densities, strains, and strain-rates. In this technical report our primary goal is to calibrate a PTW model of beryllium strength for strain-rates involved in flyer-plate impact experiments.

Prime, Adams, and Chen [1] give an overview of two strength models used to model beryllium flyer-plate shock data collected at Technical Area 55 (TA-55) at LANL. The shock data consists of six velocity wave profiles from shot pressures ranging from $20 - 200\,kbar$. First, they compare previous calibrations of Mechanical Threshold Stress (MTS) and PTW models. The paper argues that both strength models calibrations deviate from observed data during extrapolation to higher strain rate regimes. They then compare MTS and PTW fits to the six beryllium shocks with different pressures and experimental setups (impactor material, windowing, etc.). They found that though MTS and PTW had similar performance when calibrated to lower strain data when extrapolated to flyer-plate data at higher strain-rates the models gave significantly different predictions.

Armstrong [5] surveys the work done on validating beryllium strength models, using Hopkinson bar and quasi-static data for calibration and flyer plate data for validation. He sets up the underlying problem that gave rise to the current research question. That is, many calibrations of PTW models agree in modeling lower strain Hopkinson bar data but diverge significantly when extrapolated to high strain. Armstrong concludes that a PTW model calibrated by Chen provides the best agreement to flyer plate data. While these settings might be, therefore, the defensible defaults, we take a different, and comparable, model from Armstrong's survey as default values for parameters in our PTW model.

Swegle and Grady [6] discuss the interplay of strength and viscosity properties of materials when simulating shocks. The use of artificial viscosity addresses the numerical issue of modeling a discontinuous shock by smoothing the shock into a transition over multiple mesh regions. The artificial viscosity may justifiably represent the material's viscous behavior, but it also can drive erroneous solutions, as the shock rise time depends on the zone size and viscosity, so the model may be quite sensitive to these elements. They also make a clear association between strength and the slope of the hardening curve, the latter we extract from our simulations to track sensitivity

to strength parameters.

We use a type of Particle Swarm Optimizer (PSO) called a gravitational search algorithm to traverse and optimize parameter vectors in the PTW parameter space. The PSO was first introduced in [7] for the training of artificial neural network weights inside of a perceptron. Thirteen years later an adaptation called the Gravitational Search Algorithm [8] was created that emulates Newtonian physics to allow for a heuristic convergence of a cost function.

Using the GSA as an optimizer for our parameter space, along side consultation from Subject Matter Experts (SME). After optimizing the parameter space and we used the data from the GSA to preform a convergence study to find a value that allowed us to better fit the simulation data to the experimental data. The methodology of the overall experiment is explained in more detail in section 2.

# 2 Methodology

## 2.1 Scope of Analysis

Our current PTW model for Beryllium was calibrated using low strain rate Hopkinson bar and quasi-static data alongside high strain rate Flyer-plate data. The reason why we used flyer-plate data is to better fit the PTW model at higher strain rates. This allows us to optimize a subset of the parameters governing the PTW plastic deformation model. These parameters can be optimized to better fit the PTW model at higher strain rates, without affecting its fit to lower strain rate data.

In order to narrow the scope of our analysis, we isolated effects attributable to particular changes in the PTW model. Many aspects of the simulation have coupled effects that are difficult to distinguish from other modeling choices. For example, both the strength model and the equation of state (EOS) affect the simulation's fit to flyer-plate data. Therefore, calibration of one depends on the initial choice for the other.

Additionally, if multiple materials are involved in an experiment and its corresponding simulation, the parameterization of one material's strength model might add an unwanted level of uncertainty into the overall simulation. An example of this would be hitting a Be plate with an impactor plate that is as soft as clay, thus eliciting a weaker response from the Be target. On the other hand, if a Be plate were struck with an impactor set to be as hard as diamond, it would elicit a stronger response. Also, different models come into play at different points along with the wave profile. Our experimental data and simulation capture the target plate's velocity for the full duration of the shock, which includes not only elastic and plastic deformation but reverse yielding and spall as well.

To mitigate these coupled effects, we used data from the homogeneous experiments with fixed parameters in the simulation for the flyer and impactor. First, while we had data from experiments using sapphire and tantalum impactors, we began our analysis with the experiments that used Be for both impactor and target (shot $55-429$ and $55-430$) in Section 1.2, Table 1. These two experiments differ in their impactor/target width and impact velocities but have only one material, beryllium. Thus, for these simulations, we knew our calibration would be independent of modeling choices for other materials made outside the scope of our study since no other materials were involved. However, we did not limit our work to just the Be/Be shots, and incorporated multi-material impactor data, but did not fully explore the complicating effects of tantalum and sapphire modeling choices. We leave decoupling material model choices to future work.

Next, we calibrated the simulation to its fit, using a subset of the experimental data that was sensitive to strength. Strength has the greatest effect on the slope of the plastic rise. The steeper the slope the weaker the material is made, and shallower makes the material stronger. Therefore, we calculated the root mean squared error (RMSE) between the experimental data and simulation from zero seconds to the time at which the target reaches its peak velocity, a time unique to each shot. The reverberations in the velocity past the peak are sensitive to the damage, rather than strength, model, so including that region in the RMSE calculation would mean we were calibrating to features strength should not influence on.

Finally, we fixed both the EOS and damage models for our calibrations. We used a sesame table with no damage model for all simulations. This choice ensured that we could attribute the effects we saw to changes in the PTW strength model, interactions between these models should be examined, however we leave this decoupling for future work.

Most importantly, PTW's model form significantly narrowed the scope of our parameter calibration. While the PTW model has 11 parameters, we examined only two. This particular plastic deformation model is designed to be valid over a range of input conditions, which include strain, strain rate, and temperature. Due to the variations in experimental samples, measurement variation, as well as slight inadequacies in the model, no single parameter setting gives a good match to all of the experimental data for a given material.

The variables in the PTW Equation are as shown in table 2 and table 3:

| Parameters | | |
|---|---|---|
| Parameter | Description | Default Values |
| $\theta_0$ | Initial strain hardening rate | 0.0394 |
| $p$ | Constant modifying Voce hardening law | 2 |
| $S_0$ | Maximum saturation stress (at 0K) | 0.0077 |
| $S$ | Minimum saturation stress (melting) | 0.0006 |

Table 2: PTW parameters

| Parameters | | |
|---|---|---|
| Parameter | Description | Default Values |
| $\kappa$ | Thermal activation energy term relating to temperature | 0.145 |
| $\psi$ | Thermal activation energy term relating to strain-rate | 1.0′10⁻6 |
| $y_0$ | Maximum yield stress (at 0K) | 0.0018 |
| $y_{inf}$ | Minimum yield stress melting) | 0.0004 |
| $y_1$ | Scaling parameter for medium strain-rate regime | 0.0077 |
| $y_2$ | Exponential parameter for medium strain-rate regime | 0.16 |
| $\beta$ | Material constant used in describing the high rate sensitivity in 2nd regime | 0.16 |
| $T_m$ | Melting temperature | 1557 K |
| $G_0$ | Shear modulus (at 0K) | 152.4 109 N/m2 |
| $\alpha$ | Constant in G(T) Equation | 0.23 |
| $C_V$ | Heat Capacity | 1820 J/Kg/K |
| $A$ | Atomic weight | 1.447′10⁻26 Kg/atom |
| $p$ | Density | 1848 Kg/m3 |

Table 3: PTW parameters

## 2.2 PTW parameter selection

The PTW yield stress equation is:

$$\hat{\tau}_y = max\{y_0 - (y_0 - y_\infty) * F_{error}(\kappa \hat{T} ln(\gamma\dot{\xi}/\dot{\psi})), min\{y_1(\dot{\psi}/\gamma\dot{\xi})^{y_2}, s_0(\dot{\psi}/\gamma\dot{\xi})^{\beta}\} \quad (1)$$

which can be simplified to:

$$\hat{\tau}_y = max\{\hat{\tau}_y^L, min\{\hat{\tau}_y^M, \hat{\tau}_y^H\} \quad (2)$$

We focused on this equation and its parameters rather than both it and the PTW saturation stress equation. This decision was made because strains in flyer-plate experiments are not high enough to cause the material to reach its saturation stress, this range can only affect the yield stress.

Next, of the 11 parameters in the equation above, we hypothesize that only a small subset will affect the fits to flyer-plate data. $\hat{\tau}_y^L$ should be exercised at strain

rates reached by Hopkinson bar and quasi-static data, which are lower rates than flyer-plates reach. Therefore, changing $\hat{\tau}_y^L$ parameters should not affect the fit to flyer-plate data. In contrast, $\hat{\tau}_y^M$ is exercised at the strain rates flyer-plates reach, so perturbing its parameters should affect how strongly beryllium is modeled at these higher strain rates, and therefore the simulation fit to flyer-plate data. As a bonus, because Hopkinson bar and quasi-static experiments do not reach strain rates corresponding to $\hat{\tau}_y^M$, perturbing its parameters should not affect how strong Be is modeled at their lower strain rates, and thus not affect simulation fit to Hopkinson bar and quasi-static data. We must confirm this hypothesis in future work, because the distinction between $\hat{\tau}_y^L$ and $\hat{\tau}_y^M$ may not be as defined as described above; flyer-plate experiments exercise a range of strain rates, some of which may stray into the $\hat{\tau}_y^L$ regime, and the reverse with Hopkinson bar and quasi-static experiments extending into the $\hat{\tau}_y^M$ regime.

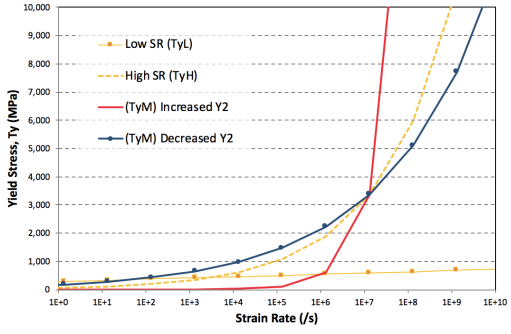


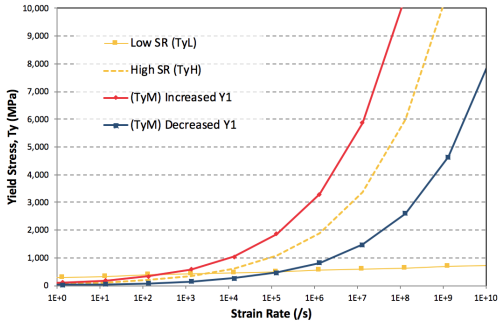


Assuming flyer-plates correspond to $\hat{\tau}_y^M$ yield stresses, we then have five parameters to examine: $y_1$,$\dot{\psi}$, $\gamma$, $\dot{\xi}$, and $y_2$. We will only examine $y_1$ and $y_2$. First, $\dot{\psi}$ is the independent variable, strain rate, and $\dot{\xi}$ is not a model parameter and is a function of other physical quantities. Next, while $\gamma$ is a model parameter, it is present in both $\hat{\tau}_y^L$ and $\hat{\tau}_y^M$, so changing it would affect the fit in both the $\hat{\tau}_y^L$ and $\hat{\tau}_y^M$ strain rate regimes. Thus, only two parameters remain to calibrate without affecting previous calibrations. Our calibration of the PTW strength model of Be using flyer-plate data will only optimize two parameters:$y_1$ and $y_2$. Calibrating these parameters will allow Be's PTW model to transition from "low" strain rates to "high" strain rates.

## 2.3 Optimization

In order to Optimize $y_1$ and $y_2$ for "high" strain rates they will be simulated and there results will be compared to flyer-plate data. While current strength models are

only calibrated using Hopkinson bar and quasi-static stress/strain data. Hopkinson bar and quasi-static experiments provide experimental data with strain rates up to several thousand per second. However, t his is considered to be in the “Low" strain rate region, while we would like to calibrate the strength models at a higher strain rate regimes. We begin our “High" strain rate PTW calibration from the parameter settings determined by PTW calibrations with Hopkinson bar and quasi-static data - these parameters should be a good default from which to start our optimization procedure. These settings are listed in Section 2.1, Table 2-3 [5].

## 2.4 Simulation

Our simulations are done with advanced simulation and computation multi-physics code developed at LANL. We simulate our flyer-plate experiment in one-dimension. This is because it allows us to limit our analysis of the wave profile before the reverberations and after peak velocity. These of which are produced by the wave rebounding off the back and sides of the target. Because of this anything other than one-dimensional calculations are unnecessary. Calculations from the “tracer", or mesh zone, at the “rear" of the simulated target are recored. This would be similar to VISAR data’s being taken from the backside of the target plate in a flyer-plate experiment. We use either the boundary tracer or the tracer one cell internal to the boundary, as sometimes boundary calculations can yield unexpected numerical issues.

Our shock simulations are inherently sensitive to artificial viscosity settings and mesh zone size. Artificial viscosity is a technique to smooth a discontinuous shock with an instantaneous jump in velocity over multiple grid cells to facilitate the computer’s numerical calculation of simulation quantities. Increasing or decreasing artificial viscosity behaves similarly to changing the material strength.

We also consider mesh size in our analysis. Using the GSA to optimize the parameter space we ran the simulations at a resolution of 25 microns after doing an informal convergence study that confirmed this resolution would be sufficient for initial investigation. We later performed a formal convergence study on the parameters of interest, $y_1$ and $y_2$, using the slope of the simulated plastic wave. See section 3.4 for more information on the convergence study.

## 2.5 Gravitational Search Algorithm

The Gravitational Search Algorithm (GSA) [8] is a heuristic optimization method that has been developed to take into account Newtonian physics to optimize a parameter space. This optimization technique uses a collection of particles that are

interconnected by gravity, mass and the laws of motion to allow for the optimal traversal of parameters through a given cost functions parameter space.

As stated in section 1.2 there are eleven parameters in the Yield stress, the two parameters we are are looking at are the $y_1$ and $y_2$ parameters. After consulting with Subject Matter Experts (SME) the bounds for each were between 0 and 4. The high level explanation of this algorithm will be discussed in the next section while the use of this optimizer in determining the optimal parameters for the PTW strength model parameters will be discussed in section 4.

### 2.5.1 Algorithm

The GSA is a heuristic optimization algorithm that leverages the laws of Gravity, Mass and Newtonian Physics to traverse a parameter space within some bounds to allow for the convergence of agent particles, each of which represents a model with some associated cost that we wish to minimize. The algorithm is as such [8]:

Assume you have a point (N) in a parameter space *PS*, the location of the point can be represented as such $N_i = [X_i^1, X_i^2, ..., X_i^{PS}]$. Given a group of particles, or a *swarm*, where N is now equal to the total number of the particles initialized and PS represents the total number of dimensions the previously defined equations (Equation 3 and Equation 4) are used to generate how the particles interact. The Mass of a particle is represented by

$$Cost_i = \frac{1}{F(N_i)} \tag{3}$$

$$Mass_i = \frac{Cost_i - Worse\_Cost(N)}{Best\_Cost(N) - Worse\_Cost(N)} \tag{4}$$

$$Mass_i = \frac{Mass_i}{\sum_{j=0}^{N} Mass_j} \tag{5}$$

- $F(N_i)$: The value of the cost function at the point of a given particle
- $Worse\_Cost(N)$: The point in the swarm with the "Worse" cost
- $Best\_Cost(N)$: The point in the swarm with the "Best" cost
  - A minimization problem sets Best_Cost to the smallest cost in the swarm and the Worse_Cost to the largest cost in the swarm
  - A maximization problem sets Best_Cost to the largest cost in the swarm and the Worse_cost to the smallest one in the swarm

The agents need to move towards each other over time, thus we can state that at the current time, $T$, the force of gravity on a single point ($F_i(T)$) is equal to the following function:

$$F_i(T) = \sum_{i=0 j \neq i}^{N} \frac{M_i(T) * M_j(T)}{R_{i,j}(t) + \epsilon} * (N_j(T) - N_i(T)) \tag{6}$$

$$G(T) = G_0 * e^{-\alpha \frac{t}{T}} \tag{7}$$

$$F_i(T) = F_i(T) * G(T) * rand_{[0,1]} \tag{8}$$

and the acceleration at time $T$ is:

$$A_i(T) = \frac{F_i(T)}{M_i(T)} \tag{9}$$

To determine the new location of the particle we can state that its velocity is a function of the newly calculated velocity and its current acceleration.

$$V_i(T+1) = rand_{[0,1]} * V_i(T) + A_i \tag{10}$$

Now that a velocity is assigned to the particle, the new position is

$$N_i(T+1) = N_i(T) + V_i(T+1) \tag{11}$$

Our team has decided to use a Gravitational Search algorithm for the following reasons:

1. have a better understanding of the overall parameter space
2. decrease the chance of converging at a local minimum

A key difference between GSA and a simpler optimizer, such as gradient descent, is that the GSA has collaborative partners helping to search the overall parameter space. A pitfall for gradient descent is that it can fall into a local minimum; the GSA has a lower chance of falling into a local minimum because the other particles still have a chance of falling into a lower minimum in the parameter space. From there it can pull the other particle out towards the new minimum. This has a probability of continuously happening, while it is impossible for the gradient descent to follow.

## 2.6 Parameter Study

To optimize the PTW parameters ($y_1$ and $y_2$) we created a script to submit a series of jobs for a set of ($y_1$ , $y_2$) pairs, which would yield a corresponding simulation for each pair. After the simulation was complete we would assign each pair a score. This

score, (commonly known as a cost function) was given by the Root Mean Square Error (RMSE) of the simulated data to the experimental data. The goal of the GSA is to minimize the cost function; at each iteration, the particle with the lowest cost is saved as the "global minimum". As the iterations progress and the particles move around the parameter space, we hypothesize that we can find a $y_1$ and $y_2$ pair such that the simulation best overlays the experimental data and produces a single point in the parameter space that holds the optimal value.

We calculated the RMSE for each simulation in each iteration by extracting the time at which peak velocity was reached in the experimental data and retaining only the simulated and experimental data before this time. Our first RMSE calculation also excluded times before the end of the elastic precursor, aiming to isolate fit to the plastic wave, but we later decided to include all times from time zero to peak velocity, as the “end" of the elastic precursor was a subjective measurement done by eye, as opposed to the maximum velocity, which is unique. Thus, the RMSE quantified the fit to both the elastic precursor and plastic wave, the former being less obviously linked to strength; future work could investigate the sensitivity of the elastic precursor to strength.

After subsetting the data, we then interpolated the simulation to have simulated velocities at the experimental measurement times. We then found the difference in simulated and real velocity at each of these times and calculated the root of the squared distance. This procedure was done for each shot, which each had a different time of peak velocity.

Our team ran the optimizer to explore the ($y_1$ , $y_2$) parameter space for each shot separately. With this procedure, we hoped that the optimal pairs we found to be optimal would be common among, and not unique to, each shot. The outcome of all simulations sharing a common optimal set of parameter settings would imply that Be's strength model behaved similarly compared to different experiments, which would be ideal, as we would like to build a model of Be's behavior that is independent of the experimental setup. As discussed in the Results section, we found consistent behavior between the two shots (shot $55-429$ and $55-430$).

# 3 Results

## 3.1 RMSE and Implications

After using the GSA to traverse the parameter space, we plotted the history of the optimizer. This consists of every particles positional value in the parameter space and its corresponding cost. Combining multiple swarms yields dozens of position/cost pairs for each optimizer. We take these pairs and plot them in the parameter space (seen in figure 1 and figure 2).

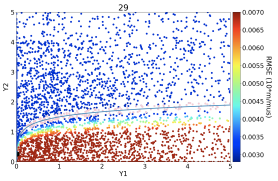


Figure 1: Shot55_429

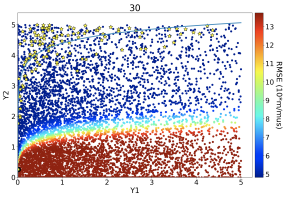


Figure 2: shot55_430

These plots allow us to get a sense of the overall parameter space, and the simulation's sensitivity of the two parameters. In both plots, each point has a different color, and position. The points color represents the RMSE (compared to the real experimental data), and its position is the ($Y_1$, $Y_2$) parameter value for the simulation. The red points indicate high RMSE and poor fit, while the blue points indicates lower RMSE (and, usually, better fit). Upon reaching its maximum iterations, each optimizer provided a global optimal point.

In figure 1 the best values identified by different GSA optimizers have been highlighted. This shows that the optimizers does no find one global optimum; rather, it settled inside an optimal region (highlighted pink). To better visualize this the same points have been plotted in 3-D (figure 3) where the Y-axis is the cost.

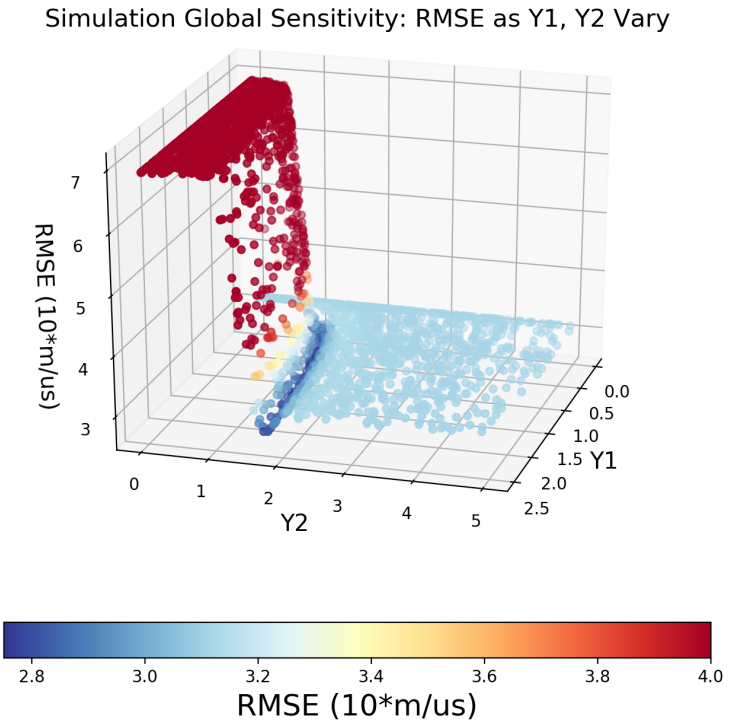


Figure 3: RMSE Plot shot55_429
RMSE graph

We can see that the sensitivity of the simulation to $Y_1$ is very low. While $Y_2$ is very sensitive where the drop off is. The optimal parameters values for our simulation can be found in the curve of the 3D plot at the trough (dark blue).

We hypothesized that there may be a global optimum somewhere within that minimal region that could be found by traversing the subset of the parameter space and increasing the simulation resolution.

Observing the logarithmic shape of the optimal region in the $Y_1$, $Y_2$ plain. We ran a logarithmic regression on the optimal values to get a line of best fit. Then generated $Y_1$, $Y_2$ points along that line of best fit and re-ran the simulation and RMSE calculation for each of those points. We found that none of these RMSE scores was significantly better than any of the others. We concluded there was no obvious, defensible single optimum ($Y_1$, $Y_2$) pair, but many which provided a better fit to experimental data at this resolution.

To choose one ($Y_1$, $Y_2$) pair from the multiple optimum values in the minimal

region, we followed a common choice in the literature. For calibrations of strength models for other materials, researchers would commonly set $Y_1 = S_0 = 0.01142$, a parameter in $\hat{\tau}_y^H$ [9]. Fixing $Y_1$ at this value, we could vary $Y_2$ and find the minimal point, likely where the $Y1 = S_0$ line crossed the minimal curve. For example, for $shot\_429$, we found $Y_1 = S_0 = 0.01142, Y_2 = 0.45$ provided the smallest RMSE for that fixed $Y_1$ value at 25 micron resolution.

## 3.2 Drawbacks of RMSE

After exploring the parameter space and the simulation's sensitivity based on RMSE, we realized that the RMSE is a non-optimal metric. Our RMSE calculation does not take into account measurement uncertainty and obscures the response of specific simulation features to parameter perturbations. These measurement uncertainties are shown below in figure 4, 5, 6 and 7.

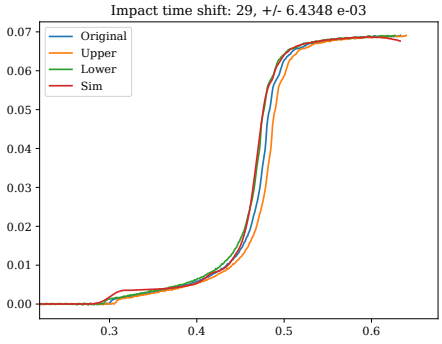


Figure 4: Shot55-429 error

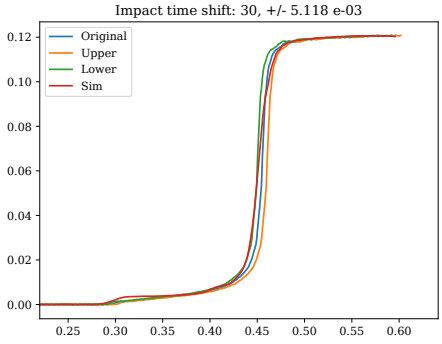


Figure 5: shot55-430 error

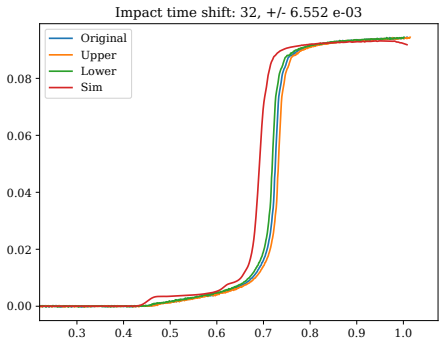


Figure 6: Shot55-432 error

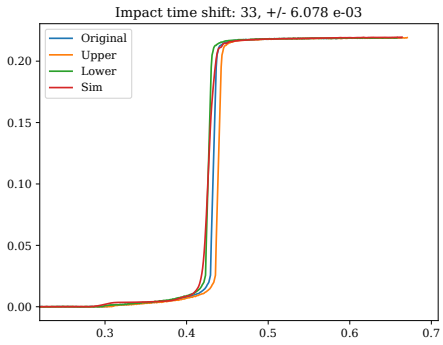


Figure 7: shot55-433 error

Taking into account that our experimental data comes in a raw measurement form that must be shifted in time by the impact time measurement, that of which is taken separately during the experiment. We know that the experimental time measurements exist in a range rather than at an exact point.

To better visualize this experimental data range we shifted each shot backward and forwards in time by the amount of the impact time error and compare it to one of the best simulations for that shot. We see changes in the RMSE value for that simulation depending on the experimental data. Looking across all shots, we see an improvement in RMSE as we shift the time measurements backward.

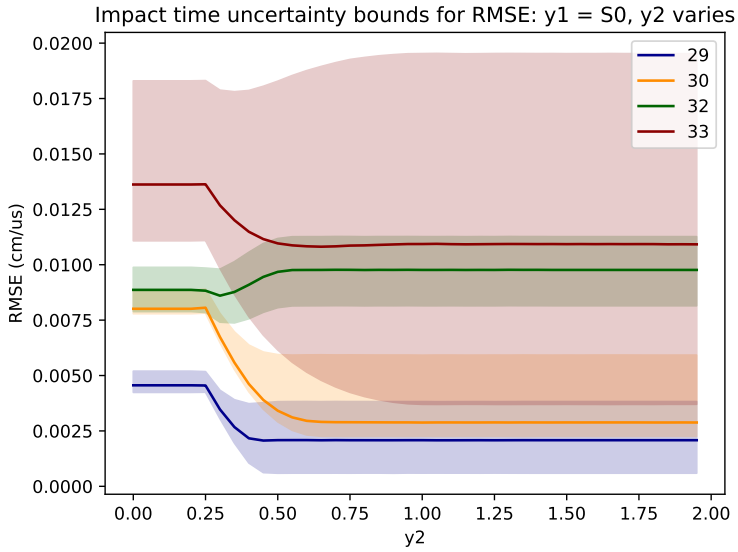


Figure 8: Error for shots

Figure 8 shows the change in RMSE when $Y_1$ is fixed and $Y_2$ increases from zero for each shot. Generally, the RMSE decreases as $Y_2$ increases. The bands are generated by creating the same RMSE curve for experimental data shifted backward and forwards in time. Across all shots, shifting the data backward improves the fit to simulation.

Our RMSE metric provides one number to approximate how well the simulation matches the entire curve equally - the arrival, elastic precursor, plastic wave, all the way to the target's peak velocity. We may not care equally how the simulation fits all points along the curve.

To remove this experimental uncertainty with respects to time we adjust our new metric to be the comparison of the slope after the elastic precursor, up to the max velocity of the simulation. This metric has the clearest interpretation in terms of strength. Shallower if the material is "harder", steeper if it is "softer". We quantify how much this feature in the simulation changes as our parameters change.

## 3.3 Slope and Experimental Uncertainty

Looking at the slope of the experimental and simulated data between the region after the elastic precursor, up to the max velocity of the output is our new metric. This new metric averts experimental uncertainty and allows us to compare the simulated

data with the experimental data. This is because the slope of the plastic wave in the experiment does not change as we shift the curve forwards and backward in time.

By sampling points in the center of this region, we can approximate the linear slope of both the simulated and experimental plastic wave. In figures 9 and 10, we filter the simulated data points to only those that fall within our designated region and interpolate a line of best fit. From there we extract the slope of the line of best fit.

These bounds are fixed even as the simulation changes, as they are based on the experimental data and we want to compare the simulation as it reaches those velocities. For example, for $shot55 - 429$, we kept simulation points where the velocity was between 0.02 and 0.05 $\frac{mm}{us}$. The plots below demonstrate our ability to approximate the slope for different simulations, as well as our experimental data.

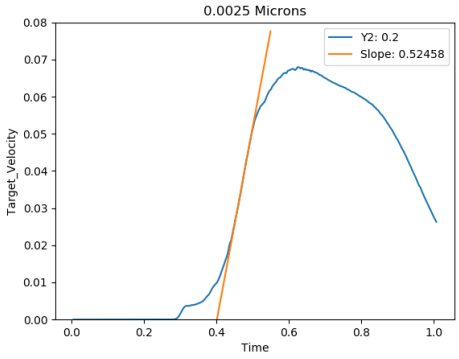


Figure 9: Shot55-429 25 micron mesh $Y_2 = .02$

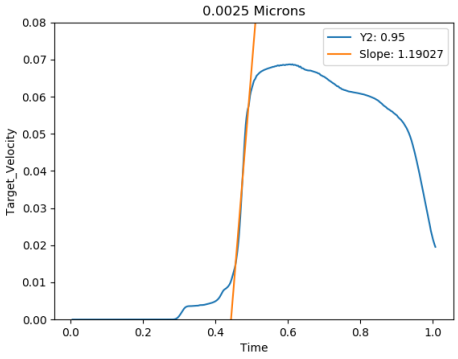


Figure 10: shot55-429 25 micron mesh $Y_2 = .95$

## 3.4 Slope and Convergence

In an attempt to understand how the given $Y_1$ and $Y_2$ values affect our simulation data, we plotted graphs of the $Y_1$ and $Y_2$ values increasing independently. As we iterate over $Y_1$ with $Y_2$ being held constant (seen in the figure below) we observed that the RMSE increases and then asymptotes. The opposite is observed for $Y_2$ with $Y_1$ held constant.

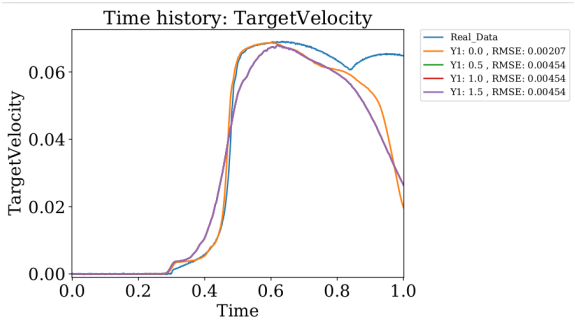


Even though the $Y_2$ value is shown to be more sensitive to change and decreases the RMSE, the fact that the data holds experimental uncertainty forces us to use a different metric for assigning a cost for the parameter pair. As previously stated, the metric we will move towards is the slope of the region after the elastic precursor, up to the max velocity of the output.

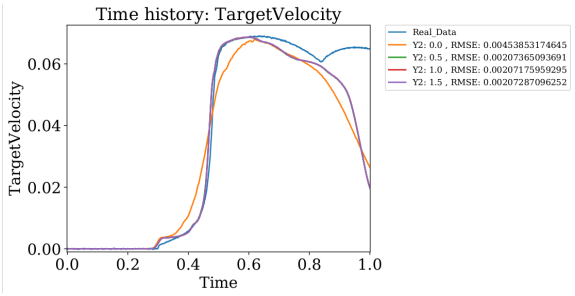


Using this metric we increase the resolution of our simulation and see where the experimental slope intercepts the simulated data. One example is shown below, For a given zone size (25 microns), when $Y_1 = S_0$ and $Y_2 = .95$ we can see that the slope of the area of interest is about 1.19. However, if we keep the resolution and $Y_1$ the same but perturb $Y_2$ we see the slope changes to about 5.3. If we continuously do this at different resolutions the graph below is generated where the horizontal line is the experimental slope.

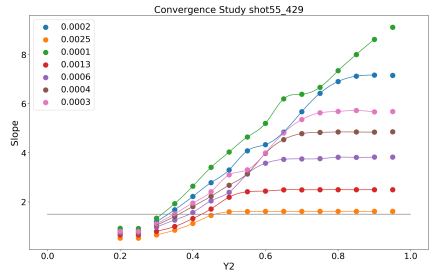


Figure 11: Convergence of shot55-429 at different resolutions

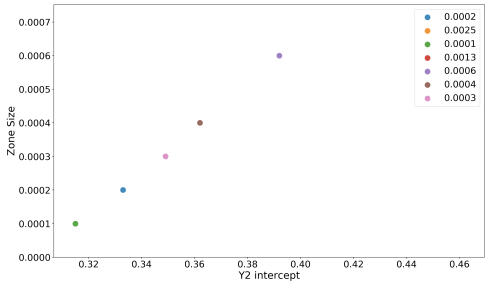


Figure 12: Interception of slope for shot55-429 at different resolutions

If we cycle through the interpolated line and plot the point that passes the experimental slope we can create a plot of "optimal" $Y_2$ values for a given resolution. From here we can extrapolate to the optimal $Y_2$ for the smallest zone size. We extrapolate the data from the lowest two-zone sizes and observe that the optimal $Y_2$ would be .297 (rounded to the nearest thousandth); to test this new optimal we ran two simulations, one at the optimal $Y_2$ and another at a different $Y_2$ to see how they compare. As expected the optimal $Y_2$ is visually the closest to the experimental data.

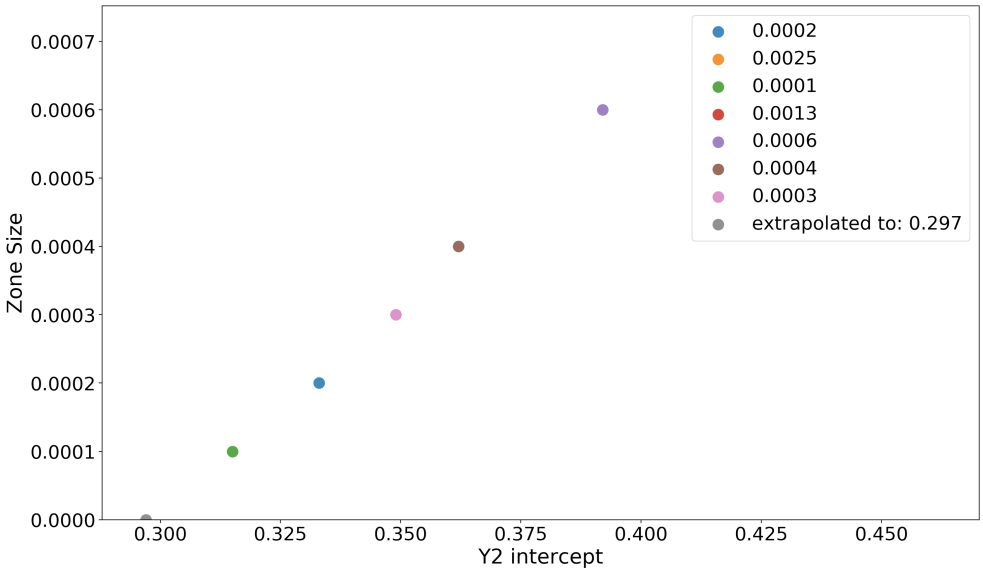


Figure 13: Extrapolated point for 0 micron resolutions

# 4 Conclusions

## 4.1 Findings

Through this research, we find that there is not one optimal parameter set, but rather many comparable choices for the parameters. Along the minimal curve shown in figure 3, there are a multitude of points that can be used as “optimal" points. However, if we look at the data provided we have identified, a $Y_1$, $Y_2$ pair that improve the fit to experimental flyer-plate data.

Furthermore, we found that the overall fit to high impact experimental simulations that reach $10^6 s^-1$ is less sensitive for $Y_1$ but extremely sensitive to $Y_2$. While we are unsure which $Y_1$, $Y_2$ pair will retain as the default for the CMF, our recommendation is $Y_1 = S_0$ and $Y_2 = 0.297$. The simulation data at the default parameter and the optimal parameter are shown below. As we can see for each of the shots our parameters fit better than the default values.

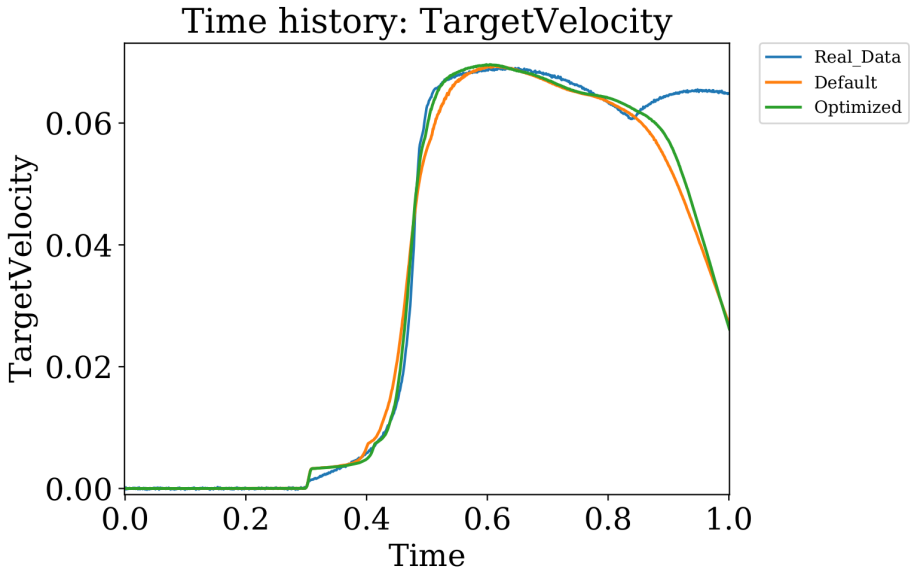


Figure 14: Default simulation vs Optimal simulation for shot55-429

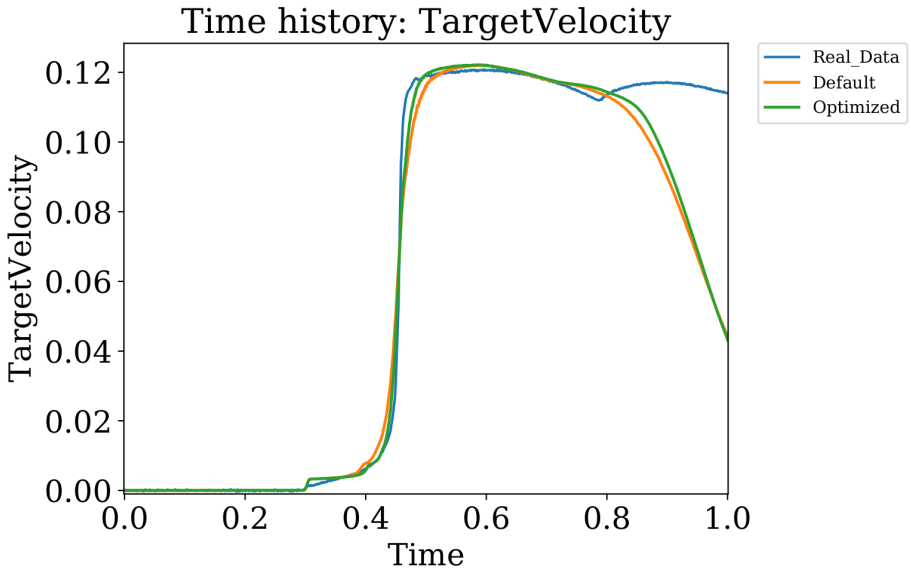


Figure 15: Default simulation vs Optimal simulation for shot55-430

We learned that the metric of extracting and comparing the experimental and simulated plastic wave slope avoids complications from measurement uncertainty, and has a more useful physical interpretation than overall RMSE. The points used to interpolate a line of best fit should be midway between the elastic precursor and the highest velocity, or near the location where the concavity changes.

In terms of implications for modeling Be, we were surprised that Be's strength appears lower in this regime than was expected. From similar work with other materials, we expected the strength to keep increasing with strain rate, as it does for those other materials. Instead, the default parameter settings from previous PTW calibrations used lower strain rate QS and HB data made Be too strong when compared to FP data. The simulated wave had too shallow a slope, and changing $Y_1$ and $Y_2$ increased the slope ( decreasing the strength) to better fit the experimental data.

## 4.2 Next Steps

To continue this work, future researchers should first redo the GSA optimization with an improved cost function. It may be optimal to build a function that is a weighted sum of RMSE and the difference in experimental slope. For example, given $\beta_1$ and $\beta_2$:

$Cost = \beta_1(RMSE) + \beta_2(slope_{exp} - slope_{sim})^2$

This weighted sum would allow the researcher to increase $\beta_2$ to emphasize fitting the slope, but also retain the ability to optimize overall fit.

We also recommend creating a scatter plot of $Y_1$, $Y_2$, and slope differences that classify points as falling within an acceptable bound of closeness to the experimental slope, below the experimental slope, and above it. This coloring would help us identify optimal regions within which to re-run the optimizer or to run a convergence study within this optimal region.

Lastly, there are statistical methods that might inform a global calibration of all PTW parameters using all available data [10]. While the parameters should have sensitivities that vary based on the strain rate regime and the $\hat{\tau}_L$ parameters shouldn't affect FP fit, we have not varied them to confirm this. It would be interesting to vary all 11 parameters using an experimental design to optimally explore the variability in the parameter space to see which parameters truly are sensitive or insensitive for FP data.

# References


[1] M. B. Prime, S.-R. Chen, and C. Adams, "Advanced plasticity models applied to recent shock data on beryllium," in *AIP Conference Proceedings*, vol. 1426, pp. 1035–1038, AIP, 2012.

[2] W. Blumenthal, S. Abeln, D. Cannon, G. Gray III, and R. Carpenter, "Influence of strain rate and temperature on the mechanical behavior of beryllium," in *AIP Conference Proceedings*, vol. 429, pp. 411–414, AIP, 1998.

[3] C. D. Adams, W. W. Anderson, G. T. Gray III, W. R. Blumenthal, C. T. Owens, F. J. Freibert, J. M. Montoya, and P. J. Contreras, "Spall and damage behavior of s200f beryllium," in *AIP Conference Proceedings*, vol. 1195, pp. 509–512, AIP, 2009.

[4] D. L. Preston, D. L. Tonks, and D. C. Wallace, "Model of plastic deformation for extreme loading conditions," *Journal of applied physics*, vol. 93, no. 1, pp. 211–220, 2003.

[5] D. E. Armstrong, "A report on the validation of beryllium strength models," tech. rep., Los Alamos National Lab.(LANL), Los Alamos, NM (United States), 2016.

[6] J. Swegle and D. Grady, "Shock viscosity and the prediction of shock wave rise times," *Journal of applied physics*, vol. 58, no. 2, pp. 692–701, 1985.

[7] R. Eberhart and J. Kennedy, "Particle swarm optimization," in *Proceedings of the IEEE international conference on neural networks*, vol. 4, pp. 1942–1948, Citeseer, 1995.

[8] E. Rashedi, H. Nezamabadi-Pour, and S. Saryazdi, "Gsa: a gravitational search algorithm," *Information sciences*, vol. 179, no. 13, pp. 2232–2248, 2009.

[9] M. B. Prime, W. T. Buttler, M. A. Buechler, N. A. Denissen, M. A. Kenamond, F. G. Mariam, J. I. Martinez, D. M. Oró, D. W. Schmidt, J. B. Stone, *et al.*, "Estimation of metal strength at very high rates using free-surface richtmyer–meshkov instabilities," *Journal of Dynamic Behavior of Materials*, vol. 3, no. 2, pp. 189–202, 2017.

[10] D. J. Walters, A. Biswas, E. C. Lawrence, D. C. Francom, D. J. Luscher, D. A. Fredenburg, K. R. Moran, C. M. Sweeney, R. L. Sandberg, J. P. Ahrens, *et al.*, "Bayesian calibration of strength parameters using hydrocode simulations of

symmetric impact shock experiments of al-5083," *Journal of Applied Physics*, vol. 124, no. 20, p. 205105, 2018.